JOURNAL OF Materials Feature Article CHEMISTRY

The route to CMR manganites: what about charge ordering and phase separation?†

B. Raveau, M. Hervieu, A. Maignan and C. Martin

Laboratoire CRISMAT, UMR 6508 associée au CNRS, ISMRA, 6 Boulevard du Maréchal Juin, 14050 Caen Cedex, France

Received 25th April 2000, Accepted 12th June 2000
First published as an Advance Article on the web 6th October 2000

The CMR manganites $Ln_{1-x}A_xMnO_3$ with the perovskite structure form a very important family of magnetic oxides, studied for their fascinating colossal magnetotransport properties. In this review, we discuss two phenomena, charge ordering and phase separation, which are crucial for the appearance of CMR in these oxides. We propose a new route to CMR, based on the Mn-site doping of these materials by other cations, such as Cr, Co, Ni and Ru.

The discovery of magnetoresistance properties in manganese oxides with the perovskite structure has allowed new features related to charge ordering and electronic phase separation to be evidenced and discussed. The properties of charge ordering in perovskite manganites $Ln_{1-x}A_xMnO_3$ (Ln = lanthanide, A = Ca, Sr) were established a long time ago,[1,2] long before the discovery of colossal magnetoresistance (CMR) effects[3–5] in these oxides.

In these systems, the charge ordered (CO) state is insulating and either antiferromagnetic or paramagnetic, but plays a very important role in the CMR effect: it can be melted into a ferromagnetic (FM) metallic state by application of a magnetic field. This ability to generate a FM metallic state is explained by a double exchange (DE) mechanism,[6] but the origin of the melting of the CO state under a magnetic field, the relationships between this transformation and the structure and chemical bonding are still matters of discussion. In a similar way, the behavior of orbital ordering and its relation with charge ordering are, so far, not completely understood.

The results obtained by numerous authors clearly show that the CMR effect results from the coexistence of two competing phases, a ferromagnetic metallic (FMM) phase with an antiferromagnetic insulating phase (AFMI).[7] It has been proposed that the intriguing properties of CMR manganites are due to electronic phase separation, involving the coexistence of regions of different carrier concentrations within the same crystal.[8] Such a pure electronic phase segregation is difficult to explain over a large length scale. In fact, it will be shown further that this phase separation originates from the coexistence of different structures within the same crystal, in agreement with the numerous structural transitions observed in these oxides.

In this review, we discuss the main features which govern the charge and orbital ordering in manganites in connection with their magnetoresistive properties, and we describe the different results which evidence phase separation in these systems.

Structural evidence for charge ordering

The first evidence for the collapse of a charge ordered state under a magnetic field was shown for $Pr_{1/2}Sr_{1/2}MnO_3$.[9] Unfortunately, subsequent structural investigations, coupling neutron diffraction and electron microscopy[10] did not confirm the existence of a CO state for this phase at low temperature. Thus, this phenomenon, although it is of particular interest, cannot be attributed to the collapse of charge ordering, but rather to a structural transition of a different nature, implying a transition from A-type AFM[10,11] to FMM upon the application of a magnetic field. In contrast, CO has been observed by structural techniques in several CE-type AFM half doped manganites $Ln_{0.5}Ca_{0.5}MnO_3$ with Ln = La, Nd, Pr, Sm.[12–16] In the CE-type AFM structure, zig-zag FM chains of Mn^{3+}/Mn^{4+} are AFM coupled with their nearest neighboring chains. In these CO oxides, a doubling of one cell parameter, a, when cooling the material below T_{CO} is observed. This behavior corresponds to a 1 : 1 ordering of the Mn^{3+} and Mn^{4+} species. From the TEM observations, it appears probable that the CO appears as Mn^{3+} and Mn^{4+} stripes which alternate along $\boldsymbol{a}$. In fact, the CO is not limited to the particular composition $Ln_{0.5}Ca_{0.5}MnO_3$. Charge ordered stripes have been evidenced by lattice imaging in electron microscopy for $x > 0.50$ in $La_{1-x}Ca_xMnO_3$[17] and for $0.4 \leqslant x \leqslant 0.75$ in $Sm_{1-x}Ca_xMnO_3$.[15] Such phenomena are illustrated by the lattice images of the "SmCa" manganites recorded at 92 K, *i.e.* below T_{CO} (Fig. 1). For particular x values, $x = 3/4$, 2/3 and 1/2, a system of fringes spaced by 22 (Fig. 1a), 16.5 (Fig. 1b) and 11 Å (Fig. 1c) respectively, is observed, corresponding to a quadrupling, a tripling and a doubling of the $a = a_p\sqrt{2}$ parameter, in agreement with the corresponding electron diffraction patterns. These results can be easily interpreted as the alternation along a of one Mn^{3+} stripe, with three (Fig. 2a), two (Fig. 2b) and one (Fig. 2c) Mn^{4+} stripes. For intermediate x values, the situation is more complex, as exemplified by two lattice images (Fig. 3b,c) recorded for $x = 0.55$, where it is shown that the ordering of the stripes either takes place in a short range manner (Fig. 3b), or in a regular long range sequence, but with a more complex "periodicity" close to $7a_p\sqrt{2}$. In fact, whatever the value of x in the range from 0.40 to 0.75, a long range ordering of the Mn^{3+} and Mn^{4+} stripes exists, which can be either commensurate for particular x values, or incommensurate for intermediate x values. Such a long range ordering of the stripes can thus be characterized by the wave $\boldsymbol{q}$ vector, which is remarkably found to be roughly equal to the $1-x$ value, *i.e.* $q \approx 1-x$ at 92 K, so that the superstructure along a for particular x values is given by $a \approx (1/q)a_p\sqrt{2}$.

The transition from the AFM charge ordered state to the paramagnetic state is clearly evidenced by the evolution of the q value *versus* temperature, as shown for several x compositions (Fig. 4). After the low temperature plateau which characterizes the CO, the $\boldsymbol{q}$ vector decreases abruptly as T increases, corresponding to the disappearance of charge ordering above T_{CO}. Note that the T_{CO} value deduced from the structural evolution is closely connected with the T_{peak} value observed on the magnetization curves of these oxides (Fig. 5), *i.e.* $T_{peak} \approx T_{CO}$, showing that charge ordering plays a prominent role in the appearance of the AFM state at low temperature. This is the reason why many authors assign the $M(T)$ peak of

†Basis of a presentation given at Materials Discussion No. 3, 26–29 September, 2000, University of Cambridge, UK.

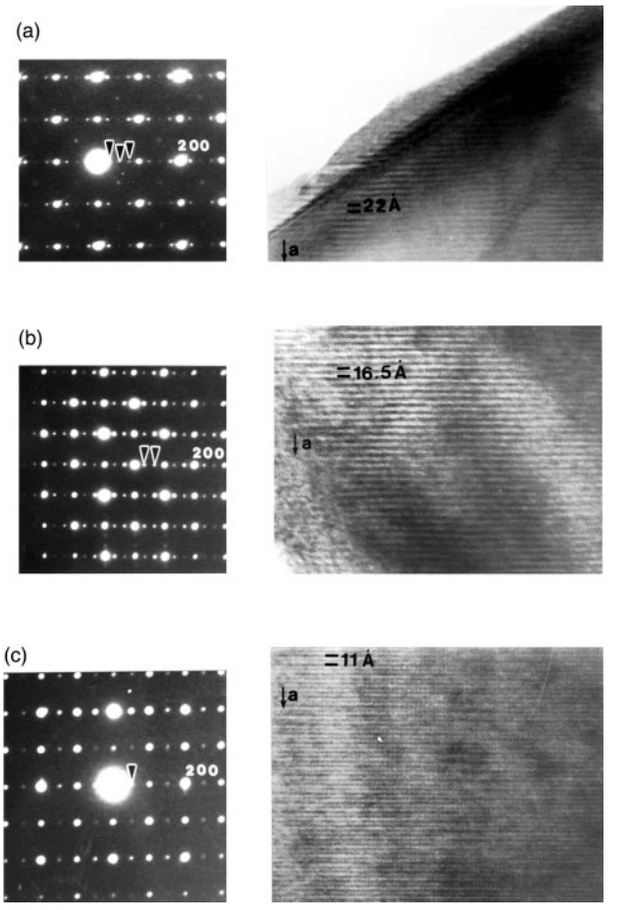

Fig. 1 [010] ED patterns and [010] lattice images recorded at 92 K for $Sm_{1-x}Ca_xMnO_3$ with (a) $x=3/4$, (b) $x=2/3$ and (c) $x=1/2$.

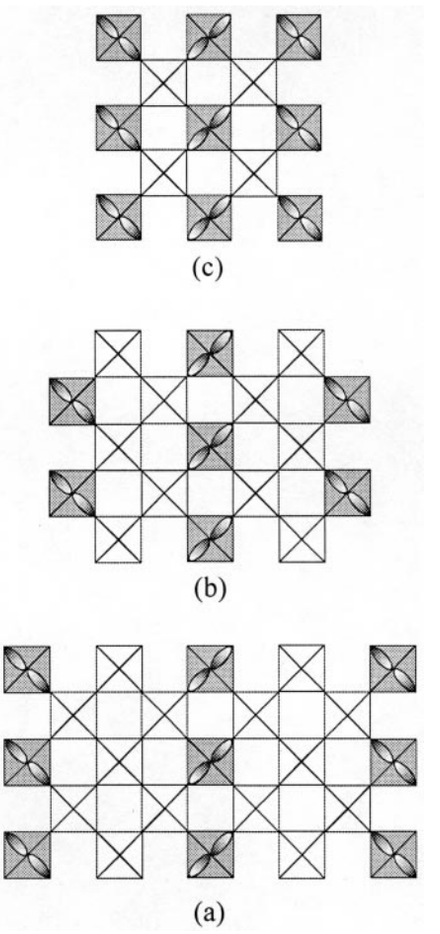

Fig. 2 Examples of structural models for $Sm_{1-x}Ca_xMnO_3$ with (a) $q=3/4$, (b) $q=2/3$ and (c) $q=1/2$.

the manganites to charge ordering, but without any crystallographic proof of its existence.

The effect of A cation size upon CO: influence on CMR properties

The strong influence of the size of the A-site cations upon charge ordering has been evidenced by several authors.[18–20] This phenomenon is easily explained by the fact that the Mn–O–Mn bond angle is significantly affected by the size of the A cations and, consequently, the e_g band width is strongly dependent on $\langle r_A \rangle$. A comparison of the magnetic phase diagrams recently established for four $Ln_{1-x}A_xMnO_3$ systems, with Ln = Pr, Sm and A = Ca, Sr,[21] illustrates the important role of the A cation size upon CO and, consequently, upon the magnetotransport properties of these oxides. The "SmCa" (Fig. 6a) and "PrCa" (Fig. 6b) manganites, which are characterized by smaller $\langle r_A \rangle$ values, exhibit both CO domains for a wide range of compositions, from $x=0.40$ to 0.80 for Sm and from 0.34 to 0.85 for Pr; their regions coincide in both cases with a large AFMI region. In both systems, T_{CO} goes through a maximum for $x=0.60$. The "SmCa" system exhibits maximum T_{CO} values significantly larger than those of the "PrCa" system, showing that T_{CO} is reinforced as $\langle r_A \rangle$ decreases when replacing praseodymium by samarium. Such an increase of T_{CO} by decreasing $\langle r_A \rangle$ was also shown for the solid solution $Pr_{0.5}Sr_{0.5-x}Ca_xMnO_3$,[20] for which T_{CO} increases from 180 K for $x=0.25$ to 250 K for $x=0.50$. Note that the charge ordering temperature may be significantly different from the Néel temperature, as shown for the "PrCa system", for which $T_N < T_{CO}$ (Fig. 6b). When $\langle r_A \rangle$ increases, the CO is rapidly destabilized, as shown for the "SmSr" manganites (Fig. 6c), for which the CO domain is reduced to $x=0.4$–0.66, and finally disappears for higher $\langle r_A \rangle$ values, as illustrated by the "PrSr" system (Fig. 6d), for which no CO was evidenced. Note also that the dramatic influence of $\langle r_A \rangle$ upon T_{CO} is confirmed: the "SmSr" manganites show T_{CO} values ranging from 130 to 200 K (Fig. 6c), to be compared to the "PrCa" system (Fig. 6d), whose smaller $\langle r_A \rangle$ values allow T_{CO} values up to 260 K to be reached.

It is also remarkable, upon comparing these four diagrams, that the reduction of the CO region, which results from the increase of $\langle r_A \rangle$ (Ca→Sr), takes place to the benefit of the ferromagnetic domain, which expands from $x \approx 0.04$–0.30 for the Ca systems (Fig. 6a,b) to $x \approx 0.1$–0.50 for the Sr system (Fig. 6c,d), T_C increasing with $\langle r_A \rangle$ and the FMM state replacing progressively the FMI state as $\langle r_A \rangle$ increases. Another point concerns the disappearance of the CO state on the Mn^{4+} rich side ($x>0.50$) for higher $\langle r_A \rangle$ values, *i.e.* in the Sr systems, for which an AFMI state without CO extends over a wide compositional range, from 0.60 to 0.9 for "SmSr" (Fig. 6c) and for 0.5 to 0.90 for "PrSr" (Fig. 6d). In contrast, for smaller $\langle r_A \rangle$ values, the CO state persists over a large compositional range in the Mn^{4+} region, being replaced by a short range charge ordering around $x \approx 0.8$, leading finally to a cluster glass (CG)[22] for $x \geqslant 0.9$ (see Fig. 6a,b) in which ferromagnetic clusters coexist within the AFM matrix.

This modification of the CO state *versus* $\langle r_A \rangle$ has a great impact on the magnetotransport properties of the manganites. The resistivity of the manganites is indeed influenced by charge ordering, as illustrated by the $\rho(T)$ curves of several $Sm_{1-x}Ca_xMnO_3$ oxides (Fig. 7). For the oxides corresponding to $0.40 \leqslant x \leqslant 0.85$, a transition from a semi-metallic behavior or semi-conducting state to an insulating state as T decreases is indeed observed. All the curves (Fig. 7) show a resistivity jump at a temperature T_R, which coincides in fact with the peak

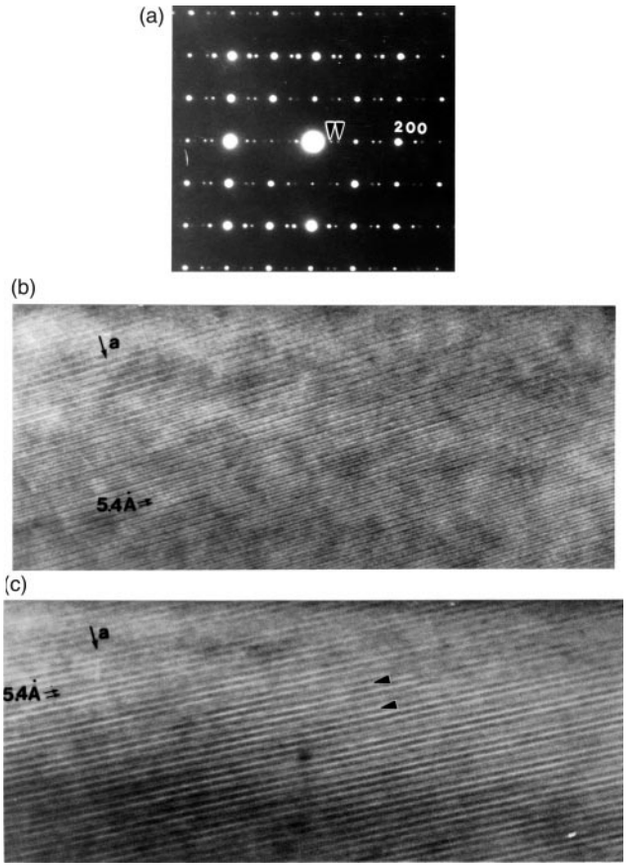

Fig. 3 $Sm_{0.45}Ca_{0.55}MnO_3$ at 92 K: (a) [010] pattern and [010] lattice images of different areas of the corresponding crystallite. They exemplify (b) short range ordering and (c) long range ordering.

temperature on the $M(T)$ curves (Fig. 5), and corresponds, in fact, to T_{CO}. Clearly, at low temperature, below T_{CO}, the antiferromagnetic insulating state is stabilized.

From the viewpoint of the CMR effect, the CO state opposes the appearance of a ferromagnetic metallic state, since it is highly insulating, but allows the obtention of the highest resistance ratio. Its destruction, by applying a magnetic field in order to get the FMM state, allows resistivity jumps of several orders of magnitude to be reached. Thus, in order to produce a CMR effect, the manganite should either exhibit a paramagnetic insulating to ferromagnetic metallic transition, or at least present a metastability of its insulating charge ordered state, which can be destroyed by a magnetic field. This viewpoint is strongly supported by comparison of the magnetic phase diagrams in Fig. 6. CMR appears in FMM regions, as shown for "SmSr" (Fig. 6c) and "PrSr" (Fig. 6d), and can extend over the CO region. For small A cations, "SmCa" (Fig. 6a) and "PrCa" (Fig. 6b) systems, CMR is obtained in spite of the absence of a ferromagnetic metallic state (FMM). CMR appears in the electron doped regions at the boundary between the CO and the CG regions. Moreover, in the hole doped region, a CMR effect can also be obtained at the boundary between the FMI and CO regions, for the PrCa system (Fig. 6b). The compositional range where the CMR appears corresponds, then, to the regions where CO is either not well established or, in any case, not yet very stable. For this reason, the CMR compositional ranges that are obtained for the small A cations are rather narrow. Nevertheless, the CMR effects are spectacular, as exemplified for the electron doped manganite[22] $Sm_{0.15}Ca_{0.85}MnO_3$ (Fig. 8a), which exhibits a resistance ratio of 10^2 at 80 K under 7 T and for the oxide $Pr_{0.7}Ca_{0.3}MnO_3$ (Fig. 8b), for which a resistance ratio of 3×10^2 at 80 K under 7 T was reached. In contrast, for large A cations, "SmSr" (Fig. 6c) and "PrSr" (Fig. 6d), the CMR effect appears only in

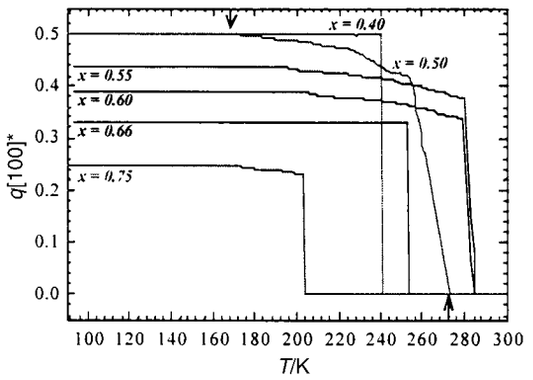

Fig. 4 Evolution of q *versus* T for the different $Sm_{1-x}Ca_xMnO_3$ samples with $0.40\leqslant x\leqslant0.75$. For the $x=0.50$ sample, arrows indicate two particular temperatures: ↑, temperature at which superlattice spot appears on cooling (T_{CO}); ↓, temperature at which the q value remains constant ($q=q_{max}$).

the hole doped region, due to the fact that the metastable charge ordered state has disappeared in the electron rich region close to $SrMnO_3$, and is replaced by a very stable AFMI state. Then, the CMR effect covers a rather wide composition range involving the adjacent CO and FMM and even FMI domains as shown for the "SmSr" system (Fig. 6c), for which T_{CO} is smaller than 200 K, so that CO state is certainly more metastable. For the largest $\langle r_A\rangle$ values, "PrSr", the CMR effect also extends over a wide composition range in the hole doped region, but, in that case, it does not result from the destruction of the CO state, but is only due to the PMI–FMM transition, which is strongly modified by the application of a magnetic field.

Phase separation: coexistence of ferromagnetism and charge ordering

The appearance of ferromagnetism at low temperature in manganites is easily explained by the DE model.[6] However, this model cannot explain the entire phase diagrams. More particularly, the role of charge ordering in the magnetotransport properties is not taken into account in the framework of double exchange. In the same way, magnetization and neutron diffraction studies evidenced weak FM moments which could not be explained by DE alone. In order to explain such features, several theoretical papers[23–25] have proposed the existence of phase separation between hole undoped antiferromagnetic regions and hole rich antiferromagnetic regions at low temperature. Arguments for the coexistence of two

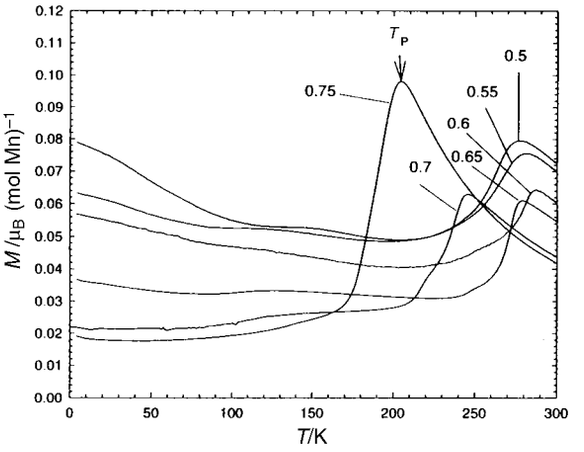

Fig. 5 T dependence of the magnetization of the series of $Sm_{1-x}Ca_xMnO_3$ samples, where T_{peak} indicates the temperature of the maximum magnetization value.

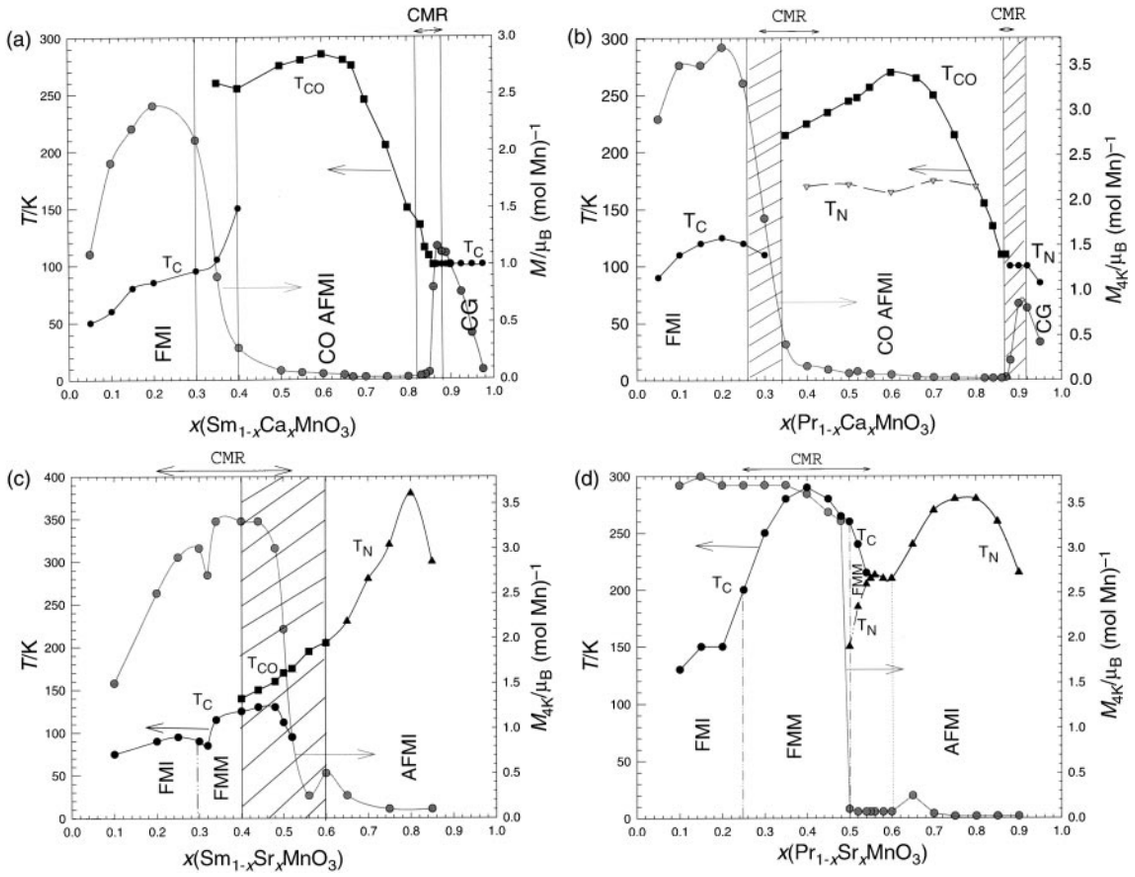

Fig. 6 Magnetic phase diagrams for the $Sm_{1-x}Ca_xMnO_3$ (a), $Pr_{1-x}Ca_xMnO_3$ (b), $Sm_{1-x}Sr_xMnO_3$ (c) and $Pr_{1-x}Sr_xMnO_3$ (d) series. The gray symbols and lines are for the magnetization values at 4.2 K (right y axis). Black symbols: (●) T_C, (■) T_{CO}, (▲) T_N. FM: ferromagnet, M for metal and I for insulator; AFM: antiferromagnet; CO: charge ordered; CG: cluster glass. The dashed areas are for intermediate regions. The CMR compositions are delimited by arrows in the upper parts.

phases, supporting the model of phase separation, were also developed in several experimental works on manganites.[26–29] The coexistence of the CO state with the FMM phase was shown, for instance, by *in situ* observation on heating a $Nd_{0.5}Sr_{0.5}MnO_3$ sample in an electron microscope.[30] This was interpreted as microscopic electronic phase separation. In a recent study of manganites, Uhera and Cheong[31] showed that the coexistence of FM and CO can be dramatically influenced by cooling rate and aging, and suggested that the origin of the phase separation is, in fact, structural.

These results demonstrate that the CO state plays a role in the transition to the FMM state, and strongly suggest that the nature of the transition under a magnetic field is percolative, so that ferromagnetic clusters within the CO-AFM matrix are formed in a first step, the sample going from an AFMI to a FMM behavior.

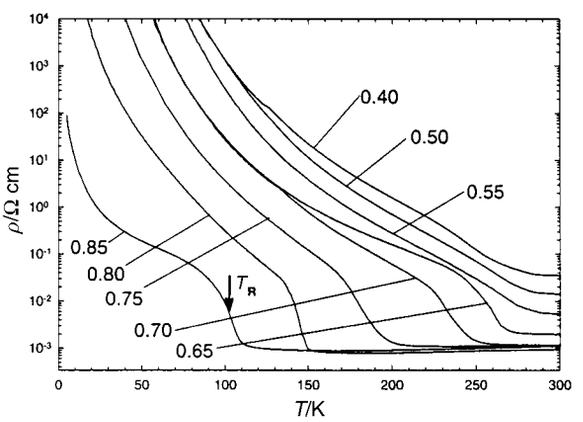

Fig. 7 T dependence of the resistivity for the $Sm_{1-x}Ca_xMnO_3$ samples with $0.40 \leqslant x \leqslant 0.85$ (x values are labelled on the graph). The arrow indicates T_R.

Mn-site doping: a chemical route to CMR

Bearing in mind the role of charge ordering in the magnetotransport properties of the manganites, it should be possible to enhance the CMR properties of these materials by weakening, or even by suppressing, the CO state using a chemical route. The doping of Mn sites with various foreign cations is, in this respect, a very efficient method, since it introduces disorder on the Mn sites and is susceptible to breaking both orbital and charge ordering.

The Mn-site doping of the charge ordered manganite $Pr_{0.5}Ca_{0.5}MnO_3$ with various M cations ($M = Mg^{2+}$, Fe^{3+}, Al^{3+}, Ga^{3+}, Ti^{4+}, Sn^{4+}) leads to destruction of the charge ordering.[32] For example, the signatures of the CO on both the $\rho(T)$ (Fig. 9) and $\chi'(T)$ curves (Fig. 10) have disappeared with only 3% dopant, and a weak ferromagnetic component is observed at low temperature on the $\chi'(T)$ curves (Fig. 10). Consequently, CMR properties are induced by doping, as exemplified for $Pr_{0.5}Ca_{0.5}Mn_{0.97}Fe_{0.03}O_3$ (Fig. 11). But the most spectacular effect is obtained by doping the Mn sites with magnetic elements, such as Cr, Co, Ni and Ru. In the series $Pr_{0.5}Ca_{0.5}Mn_{1-x}M_xO_3$ with M = Cr, Co, Ni, it is shown[33–35] that a magnetic field is not required to induce insulator to metal transitions. Clear I–M transitions are observed, in the absence of magnetic field in the Cr doped material $Pr_{0.5}Ca_{0.5}Mn_{1-x}Cr_xO_3$ for x values as low as 0.02 (Fig. 12). Correlatively, the $M(T)$ curves (Fig. 13) show that the metallic

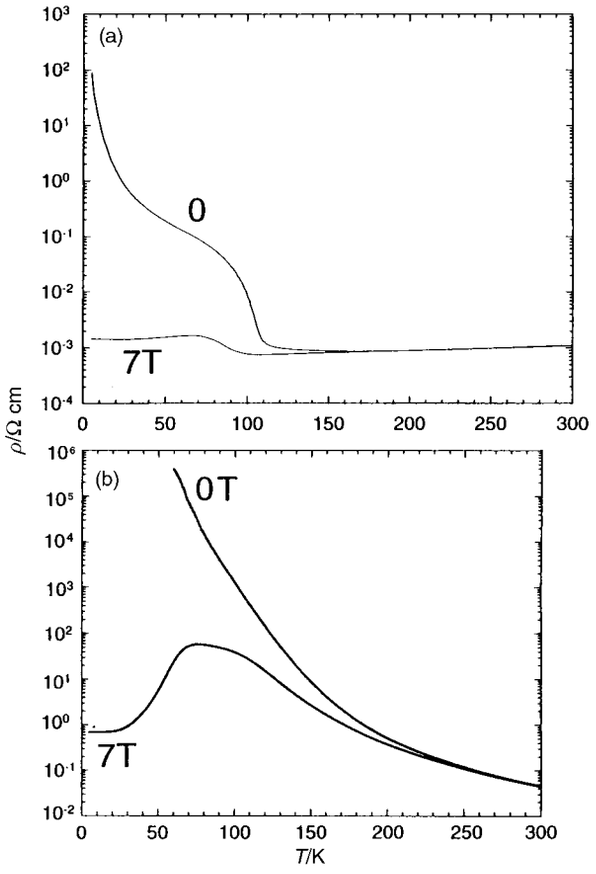

Fig. 8 T dependence of the resistivity registered under 0 and 7 T for (a) $Sm_{0.85}Ca_{0.15}MnO_3$ and (b) $Pr_{0.7}Ca_{0.3}MnO_3$.

state at low temperature is associated with ferromagnetism, large magnetization values of 3 μ_B, close to the theoretical magnetic moment, being reached. The disappearance of charge ordering by chromium doping was clearly evidenced by the electron microscopy study of $Sm_{0.5}Ca_{0.5}Mn_{0.97}Cr_{0.03}O_3$. As a consequence of the disappearance of CO, CMR behavior similar to that of the hole doped manganites, without any CO, is restored. This is illustrated in Fig. 14, where the $\rho(T)$ curves recorded at 0 and 7 T allow $Pr_{0.5}Ca_{0.5}Mn_{0.97}Cr_{0.03}O_3$ to be compared with $Pr_{0.7}Ca_{0.2}Sr_{0.1}MnO_3$. Similar results are obtained for cobalt and nickel doping, but chromium is the most efficient cation to induce ferromagnetism.

In fact, further studies of the Cr doped manganites[36,37]

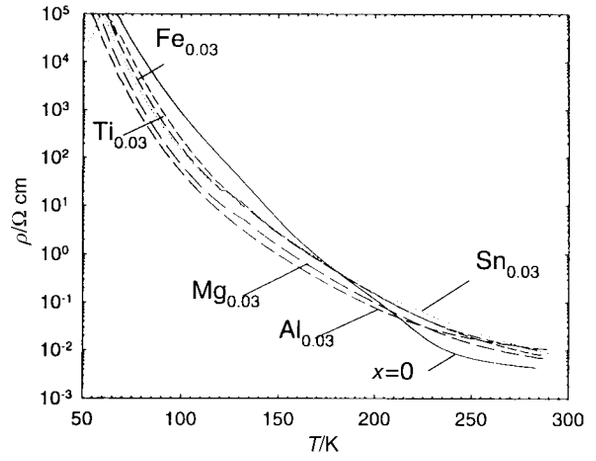

Fig. 9 $\rho(T)$ curves of $Pr_{0.5}Ca_{0.5}MnO_3$ (pristine compound) and of the corresponding doped manganites $Pr_{0.5}Ca_{0.5}Mn_{0.97}M_{0.03}O_3$ ($M = Mg^{2+}$, Al^{2+}, Fe^{3+}, Ti^{4+}, Sn^{4+}).

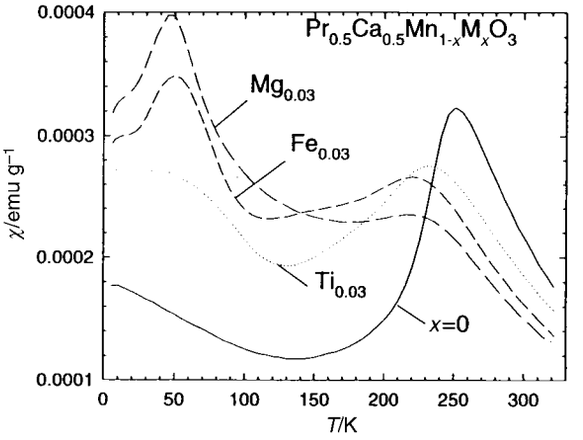

Fig. 10 Dependence of the real part of the susceptibility (χ') for $Pr_{0.5}Ca_{0.5}MnO_3$ and 3% doped $Pr_{0.5}Ca_{0.5}Mn_{0.97}M_{0.03}O_3$ samples ($M = Mg^{2+}$, Fe^{3+}, Ti^{4+}).

clearly establish that the transformation of the CO state into the FM state takes place by a phase separation mechanism. Coexistence of CO domains with the ferromagnetic metallic phase is clearly evidenced by electron diffraction at low temperature.[37] This is illustrated by the ED pattern and lattice image of the manganite $Pr_{0.5}Ca_{0.5}Mn_{0.95}Cr_{0.05}MnO_3$ measured at 92 K (Fig. 15). The [010] ED pattern (top Fig. 15) shows that the superlattice reflections are indeed in an incommensurate position ($q = 0.42$), whereas they were close to the commensurate positions ($q \approx 0.48$) in the undoped material. The lattice image (bottom Fig. 15) shows that the order is partly destroyed, *i.e.* ordered and non-ordered domains with variable sizes coexist throughout the crystal, the first corresponding to CO regions and the second being attributed to ferromagnetic regions.

These results show that magnetic ions, like chromium, not only destroy charge ordering, but also participate in ferromagnetism. In the case of chromium, the following scenario can be proposed:[37] as Cr^{3+} replaces the isovalent Mn^{3+} cation it goes with reversed spin, leading to a decrease of the magnetic moment (3.15 μ_B observed instead of 3.45 μ_B without altering the spin direction). Direct evidence of spin reversal was given by a magnetic dichroism study on the same compound.[38] The spin configuration before and after chromium doping can be schematized as shown in Fig. 16. Without chromium (top Fig. 16) the antiferromagnetic ordering is of the CE type below 170 K, with two FM zig-zag chains antiferromagnetically

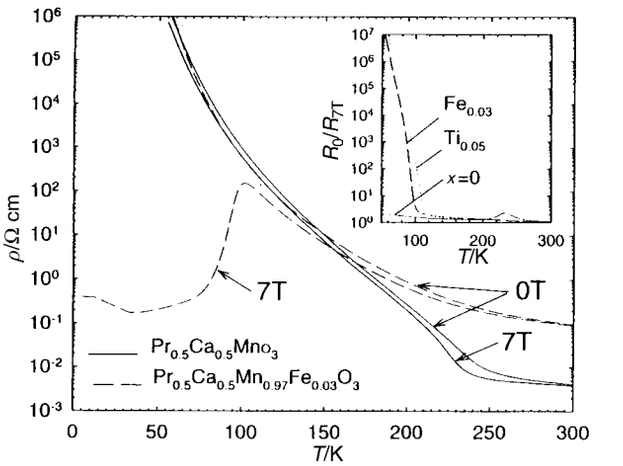

Fig. 11 Dependence of the resistivity (ρ) on T for $Pr_{0.5}Ca_{0.5}MnO_3$ and $Pr_{0.5}Ca_{0.5}Mn_{0.97}Fe_{0.03}O_3$ recorded at 0 and 7 T. Inset: dependence on T of the R_0/R_{7T} ratios, demonstrating the CMR induced by doping with M = Fe and Ti.

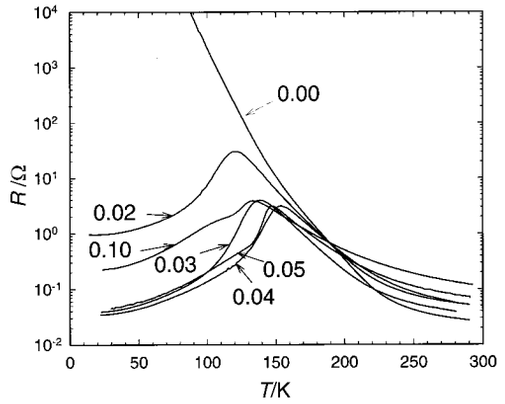

Fig. 12 $\rho(T)$ curves of the $Pr_{0.5}Ca_{0.5}Mn_{1-x}Cr_xO_3$ samples; the solid line corresponds to $x=0$.

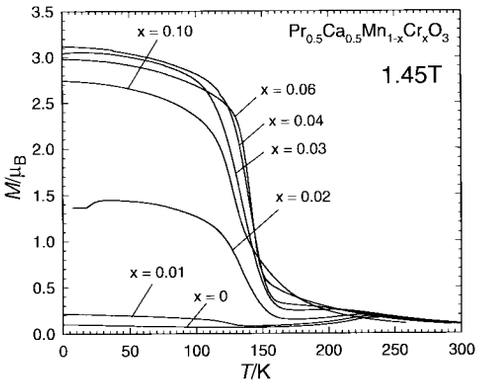

Fig. 13 $Pr_{0.5}Ca_{0.5}Mn_{1-x}Cr_xO_3$: $M(T)$ curves.

coupled in the *ac* plane, such planes are stacked along ***b*** with reversed spins. Thus, in the undoped CE-type phase, metallic conduction along the FM zig-zag chains is inhibited by the strong repulsive Coulombic interaction between the charge carriers and interchain AFM coupling. After chromium doping (bottom Fig. 16), the occupation of some Mn positions by Cr^{3+} with reversed spins breaks the AFM coupling between the chains and forms local ferromagnetic clusters (circled region at the bottom of Fig. 16). Thus, for a very small doping level ($x<0.05$), the e_g electron is itinerant within these clusters, but in the regions outside the clusters, charge and AFM ordering are weakened but still preserved. Thus, the insulating state breaks into majority CO domains, with either spins ordered antiferromagnetically or fluctuating within them, and

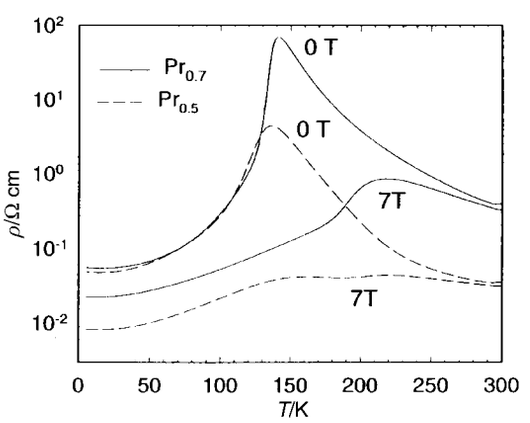

Fig. 14 $\rho(T)$ recorded at 0 and 7 T for the Cr doped $Pr_{0.5}Ca_{0.5}Mn_{0.97}Cr_{0.03}O_3$ manganite. The same curves for a classical charge delocalized $Ln_{0.7}A_{0.3}MnO_3$ manganite are also given.

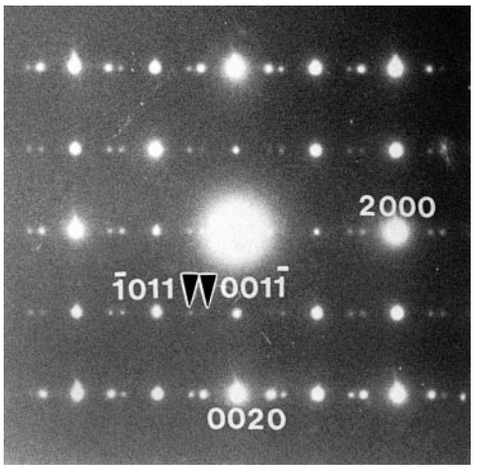

Fig. 15 [010] ED pattern of $Pr_{0.5}Ca_{0.5}Mn_{0.95}Cr_{0.05}MnO_3$ recorded at 92 K. Arrows indicate superlattice reflections.

minority ferromagnetic metallic domains. The size of the CO-AFM domains decreases as x increases and then metallicity appears in a percolative way.

The possibility of inducing an I–M transition in a CO manganite, $Nd_{0.5}Ca_{0.5}MnO_3$, by ruthenium doping was shown for the first time by Rao *et al.*,[39] the Curie temperature increasing with the ruthenium content. The doping of the Mn(IV)-rich manganites $Ln_{0.4}Ca_{0.6}MnO_3$[40] and $CaMnO_3$[41] with ruthenium shows that the potential of this cation to induce metallicity and ferromagnetism is still superior to Cr, Co and Ni. This is illustrated by the $\rho(T)$ and $M(T)$ curves (Fig. 17) of the $Pr_{0.4}Ca_{0.6}Mn_{1-x}Ru_xO_3$ series. It can be seen that, starting from an insulating phase ($x=0$, upper inset in Fig. 17), the resistivity is lowered in a spectacular way, by several orders of magnitude on doping with ruthenium, showing "double bump" curves (Fig. 17). Correlatively, ferromagnetism is induced in a spectacular way, the magnetic moment reaching a maximum value of 2.8 μ_B at 4 K for $x=0.06$ (lower inset in Fig. 17). These results show that Ru weakens charge ordering, but the disappearance of CO is not sufficient to explain the appearance of ferromagnetism and metallicity at low temperature and also the double bump phenomenon on the $\rho(T)$ curves. Again, they can be interpreted on the basis of the phase separation scenario.[23–29] For low doping levels, FM clusters are formed around the Ru cations within the AFM insulating matrix, so that, for $x=0.02$, CO coexists with these FM clusters and the resistivity is not affected significantly. For higher doping levels ($x\approx0.04$), metallic FM

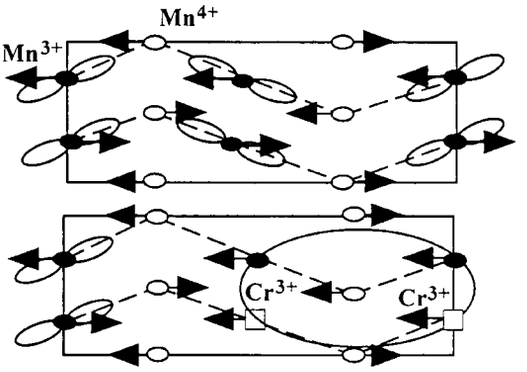

Fig. 16 Schematic spin configuration of $Pr_{0.5}Ca_{0.5}MnO_3$ (top) and $Pr_{0.5}Ca_{0.5}Mn_{1-x}Cr_xO_3$ (bottom). The dashed zig-zag lines are to illustrate interchain ferromagnetic coupling. The region enclosed by the circle represents the ferromagnetic cluster formed by two Cr^{3+} cations. Mn^{3+} e_g orbital ordering is also shown as lobes. Cr substitution weakens orbital ordering, as shown in the lower part of the figure.

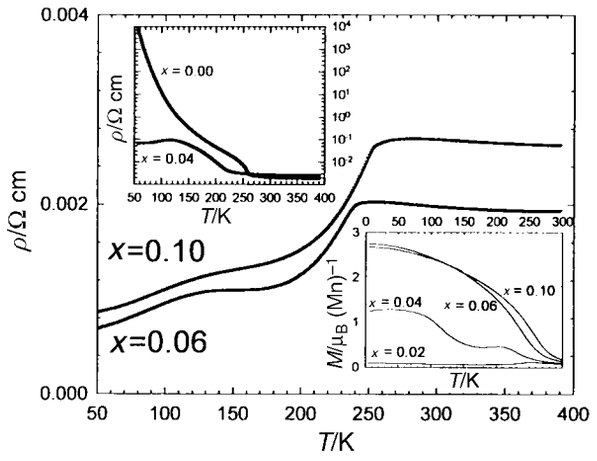

Fig. 17 $\rho(T)$ curves of $Pr_{0.4}Ca_{0.6}Mn_{1-x}Ru_xO_3$. Upper inset: $x=0$ and $x=0.04$ $\rho(T)$ curves. Lower inset: $M(T)$ curves of $Pr_{0.4}Ca_{0.6}Mn_{1-x}Ru_xO_3$.

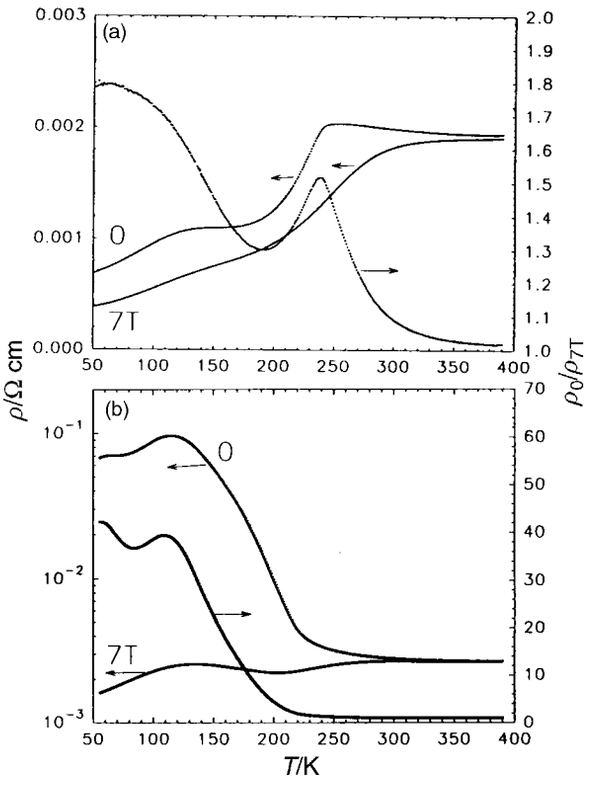

Fig. 18 $\rho(T)$ curves obtained upon cooling in 0 and 7 T (left y axis) and $\rho_0(T)/\rho_{7T}(T)$ ratio (right y axis) for $Pr_{0.4}Ca_{0.6}Mn_{1-x}Ru_xO_3$ with $x=0.06$ (a) and $x=0.04$ (b).

regions coexist with insulating AFM regions. The first bump at high temperature on the $\rho(T)$ curve (Fig. 17) corresponds to the I–M transition within the FM regions, whereas the second bump at lower temperature characterizes the competitive contribution of both regions, AFM insulating and FM metallic, to the conductivity. Finally, for $x=0.10$, the percolation of FM clusters and their large domains can be explained by the ability of this element to exhibit two high oxidation states, Ru(IV) and Ru(V). The t_{2g}^3 configuration of Ru(V) is similar to Mn(IV), whereas the t_{2g}^4 configuration of Ru(IV) is different from the $t_{2g}^3e_g^1$ configuration of Mn(III). Mn(III) can interact with both Ru(V) and Ru(IV) *via* ferromagnetic superexchange interaction involving overlap of the partly filled e_g orbital of Mn(III) and the empty e_g orbitals of Ru(IV) and Ru(V). Thus, its introduction on the Mn lattice not only tends to destroy the charge ordering, but may contribute to the increased Mn^{3+} content according to the equilibrium $Mn^{4+}+Ru^{4+}\rightleftharpoons Mn^{3+}+Ru^{5+}$. Consequently, FM clusters are generated not only by DE between Mn species ($Mn^{3+}+Mn^{4+}\rightleftharpoons Mn^{4+}+Mn^{3+}$), but also by the FM superexchange interactions between Mn^{3+} and both Ru(IV) and Ru(V). Thus, it is most probable that the FM clusters are formed around the Ru atoms, which locally destroy CO and simultaneously favor DE.

Finally, it should be emphasized that the Ru doped manganites exhibit CMR effects in spite of their metallic conductivity, as shown, for instance, for $Pr_{0.4}Ca_{0.6}Mn_{0.94}Ru_{0.06}O_3$ (Fig. 18a). More importantly, CMR is enhanced in a spectacular way for lower doping levels, when smaller FM domains coexist with AFM regions, as illustrated for $Pr_{0.4}Ca_{0.6}Mn_{0.96}Ru_{0.04}O_3$ (Fig. 18b) which exhibits a resistance ratio of 40 at 110 K under 7 T, whereas, under the same conditions, the undoped phase is not magnetoresistive. Thus, this shows that the AFM regions shrink under an external magnetic field, extending the FM clusters and eventually leading to percolation.

Concluding remarks

The few results presented in this study show the prime roles of charge ordering and phase separation phenomena in the magnetotransport properties of manganites, allowing us to explain and to discover a route to the generation of new CMR properties. Many questions, however, still need to be answered in order to understand the curious behavior of the manganites. The role of orbital ordering and its interplay with charge and magnetic ordering is one of the most important issues which has been the subject of only a few studies[13,42-43] to date. Some results suggest, for instance, that the incommensurate structure observed by electron microscopy involves the presence of partial orbital disordering and complete charge ordering, and that long range orbital ordering is never achieved so that charge order drives the orbital order at the transition. Further systematic investigations are necessary to understand all these phenomena.

References

1 E. O. Wollan and W. C. Koehler, *Phys. Rev.*, 1955, **100**, 545.
2 J. B. Goodenough, *Phys. Rev.*, 1955, **100**, 564.
3 R. M. Kusters, J. Singleton, D. A. Keon, R. H. Greddy and N. Hayes, *Physica B*, 1989, **155**, 362.
4 A. Asamitsu, Y. Moritomo, Y. Tomioka and Y. Tokura, *Nature*, 1995, **373**, 407.
5 A. Maignan, Ch. Simon, V. Caignaert and B. Raveau, *Solid State Commun.*, 1995, **96**, 623.
6 C. Zener, *Phys. Rev.*, 1951, **82**, 403.
7 M. Uhera, S. Mori, C. H. Chen and S. W. Cheong, *Nature*, 1999, **399**, 560.
8 S. Yunoki, J. Hu, A. Malvezzi, A. Moreo, N. Furukawa and E. Dagotto, *Phys. Rev. Lett.*, 1998, **80**, 845.
9 Y. Tomioka, A. Asamitsu, Y. Moritomo, H. Kuwahara and Y. Tokura, *Phys. Rev. Lett.*, 1995, **74**, 5108.
10 F. Damay, C. Martin, M. Hervieu, A. Maignan, B. Raveau, G. André and F. Bourée, *J. Magn. Magn. Mater.*, 1998, **184**, 71.
11 H. Kawano, R. Kajimoto, H. Yoshizawa, Y. Tomioka, H. Kuwahara and Y. Tokura, *Phys. Rev. Lett.*, 1997, **78**, 4253.
12 P. M. Woodward, D. E. Cox, T. Vogt, C. N. R. Rao and A. K. Cheetham, *Chem. Mater.*, 1999, **11**, 3528.
13 C. H. Chen and S. W. Cheong, *Phys. Rev. Lett.*, 1996, **76**, 4042; P. Radaelli, D. E. Cox, M. Marezio and S. W. Cheong, *Phys. Rev. B*, 1997, **55**, 3015.
14 F. Damay, Z. Jirak, M. Hervieu, C. Martin, A. Maignan, B. Raveau, G. André and F. Bourée, *J. Magn. Magn. Mater.*, 1998, **190**, 221.
15 M. Hervieu, A. Barnabé, C. Martin, A. Maignan, F. Damay and

B. Raveau, *Eur. Phys. J. B*, 1999, **8**, 31; A. Barnabé, M. Hervieu, C. Martin, A. Maignan and B. Raveau, *J. Mater. Chem.*, 1998, **8**, 1405.
16 Z. Jirak, S. Krupicka, Z. Simsa, M. Dlouha and S. Vratislav, *J. Magn. Magn. Mater.*, 1985, **53**, 153.
17 C. H. Chen, S. W. Cheong and H. Y. Hwang, *J. Appl. Phys.*, 1997, **81**, 4326.
18 N. Kumar and C. N. R. Rao, *J. Solid State Chem.*, 1997, **129**, 363.
19 A. Barnabé, M. Hervieu, C. Martin, A. Maignan and B. Raveau, *J. Appl. Phys.*, 1998, **84**, 5506.
20 F. Damay, C. Martin, A. Maignan, M. Hervieu, B. Raveau, Z. Jirak, G. André and F. Bourée, *Chem. Mater.*, 1999, **11**, 536.
21 C. Martin, A. Maignan, M. Hervieu and B. Raveau, *Phys. Rev. B*, 2000, **60**, 12191.
22 C. Martin, A. Maignan, F. Damay, M. Hervieu and B. Raveau, *J. Solid State Chem.*, 1997, **134**, 198; A. Maignan, C. Martin, F. Damay and B. Raveau, *Chem. Mater.*, 1998, **10**, 1974; A. Maignan, C. Martin, F. Damay B. Raveau and J. Hejtmanek, *Phys. Rev. B*, 1998, **58**, 2578.
23 S. Yunoki, J. Hu, A. Malvezzi, A. Moreo, N. Furukawa and E. Dagotto, *Phys. Rev. Lett.*, 1998, **80**, 845.
24 E. Dagotto, S. Yunoki, A. Malvezzi, A. Moreo, J. Hu, S. Capponi, D. Poilblanc and F. Furukawa, *Phys. Rev. B*, 1998, **58**, 6414.
25 S. Yunoki and A. Moreo, *Phys. Rev. B*, 1998, **58**, 6403.
26 P. Schiffer, A. P. Ramirez, W. Bao and S. W. Cheong, *Phys. Rev. Lett.*, 1995, **75**, 3336.
27 P. G. Radaelli, D. E. Cox, M. Marezio, S. W. Cheong, P. Schiffer and A. P. Ramirez, *Phys. Rev. Lett.*, 1995, **75**, 4488.
28 G. Allodi, R. De Renzi, G. Guidi, F. Licci and M. W. Piepper, *Phys. Rev. B*, 1997, **56**, 6036.
29 G. Allodi, R. De Renzi, F. Licci and M. W. Piepper, *Phys. Rev. Lett.*, 1998, **81**, 4736.
30 N. Fukumoto, S. Mori, N. Yamamoto, Y. Moritomo, T. Katsufuji, C. H. Chen and S. W. Cheong, *Phys. Rev. B*, 1999, **60**, 12963.
31 M. Uhera and S. W. Cheong, *Relaxation Between Charge Order and Ferromagnetism in Manganites: Indication of Structural Phase Separation*, preprint.
32 F. Damay, C. Martin, A. Maignan and B. Raveau, *J. Magn. Magn. Mater.*, 1998, **183**, 143.
33 B. Raveau, A. Maignan and C. Martin, *J. Solid State Chem.*, 1997, **130**, 162.
34 A. Maignan, F. Damay, C. Martin and B. Raveau, *Mater. Res. Bull.*, 1997, **32**, 965.
35 A. Barnabé, A. Maignan, M. Hervieu, F. Damay, C. Martin and B. Raveau, *Appl. Phys. Lett.*, 1997, **71**, 3907.
36 Y. Moritomo, A. Machida, S. Mori, N. Yamamoto and A. Nakamura, *Phys. Rev. B*, 1999, **60**, 9220.
37 R. Mahendiran, M. Hervieu, A. Maignan, C. Martin and B. Raveau, *Solid State Commun.*, 2000, **114**, 429.
38 F. Studer, O. Toulemonde, J. B. Goedkoop, A. Barnabé and B. Raveau, *Jpn. J. Appl. Phys.*, 1999, **38**, 377; O. Toulemonde, F. Studer, A. Barnabé, A. Maignan, C. Martin and B. Raveau, *Eur. Phys. J. B*, 1998, **4**, 159.
39 P. V. Vanitha, A. A. Rulraj, A. R. Raju and C. N. R. Rao, *C. R. Acad. Sci.*, 1999, **2**, 595.
40 B. Raveau, A. Maignan, C. Martin, R. Mahendiran and M. Hervieu, *J. Solid State Chem.*, in press.
41 B. Raveau, A. Maignan, C. Martin and M. Hervieu, *Mater. Res. Bull.*, in press.
42 S. Mori, T. Katsufuji, N. Yamamoto, C. H. Chen and S. W. Cheong, *Phys. Rev. B*, 1999, **59**, 13573.
43 M. Zimmermann, J. P. Hill, D. Gibbs, M. Blume, D. Casa, B. Keimer, Y. Murakami and Y. Tomika, *Phys. Rev. Lett.*, 1999, **83**, 4872.